Radiative Processes of the Solvated Electron in Polar Fluids

Neil R. Kestner*[1] and Joshua Jortner

Department of Chemistry, Tel-Aviv University, Tel-Aviv, Israel   (Received December 13, 1972)

In this paper we present a theoretical study of the physical properties of solvated electrons in ammonia based on the Copeland–Kestner–Jortner model, which incorporates short-range interactions *via* a first solvation layer and long-range interactions *via* polaron modes. We have studied bound–bound and bound–continuum optical transition emphasizing the problem of line shapes in absorption and emission. The total energy of the ground and excited states and its dependence on nuclear configurations was handled by three successive approximate calculations: (a) a temperature dependent potential including short-range radial displacements; (b) a temperature independent potential incorporating both radial and angular short-range displacements; (c) a multidimensional potential surface including both short-range and long-range (polaron) nuclear displacements. The calculated line shapes in absorption for a single solvent configuration include major contributions from short-range radial displacements and from the polaron modes. The energy and line shape for the 2p → 1s emission band is predicted. A general formula is presented for photoionization cross section including the contribution of all medium modes and in this case the role of the polaron modes is crucial.

I. Introduction

In our previous paper,[2] we advanced a model for the solvated electron in polar fluids which took into account the strong short-range interactions of the electron and the first coordination layer solvent molecules as well as the long-range interactions with the bulk medium. This model was capable of yielding quantitative information on the properties of solvated electrons in ammonia as well as providing qualitative data on excess electrons in other polar solvents. In the latter cases we did not attempt a detailed study. Recently, Fueki, Kevan and Christoffersen, in particular, have applied a similar model to study solvated electrons in water and alcohols.[3a,b] Although many questions remain concerning the trends observed in widely differing solvents[4] and solvent mixtures,[4-7] these are predicted well enough by our model to allow us to consider an entirely different set of problems, namely the details of radiative processes in which the state of the electron changes.

In this paper we will use metal–ammonia solutions as a representative system for the study of these processes. We expect the same general behavior in other polar fluids except that the relative rates of the various processes could change in different solvent systems. We will begin with a display of the latest calculations on our model[2] as well as an improved version. These new results provide a better insight into the physical properties of the solvated electron. We shall focus attention on the radiative processes of the solvated electron and, in particular, the observed absorption line shapes for bound–bound and for bound–continuum transitions as well as the yet unobserved emission line shape and the photoionization profile. The study of optical line shapes provides a starting point for the understanding of nonradiative processes of the solvated electron, such as electron capture from the conduction band to form the localized ground state, or the reverse process of thermal ionization of the ground state and of excited states. In general, the nonradiative transition probability can be expressed in terms of a generalized line shape function in the limit of zero frequency. However, in view of the special nature of the problem, where the localized

excess electron wave function is strongly dependent on the (short-range and polaron type long-range) nuclear coordinates, the theory of the optical line shapes presented herein requires a gross modification before it can be applied for the elucidation of the nonradiative decay processes of the solvated electron.

II. Calculations

A. Temperature Dependent Potentials—One-Coordinate Model. Let us briefly review the Copeland–Kestner–Jortner model[2] which incorporates the following features.

(a) We assume that in the first coordination layer around the electron there will be a small fixed number, N, of solvent molecules. In this work we will assume values of $N = 4, 6, 8,$ and 12, although the first two numbers seem to be most physically relevant.

(b) The solvent molecules in the first layer interact with the electron *via* their permanent and induced moments and with other solvent molecules in the first coordination layer *via* their repulsive forces, *i.e.*, primarily hydrogen–hydrogen repulsions and dipole–dipole repulsions.

(c) The electron interacts with the continuum beyond the first coordination layer in two ways. First of all it reacts with the inertial polarization field in the same way as in polaron theory. The use of adiabatic polaron theory is justified since we have treated the strong short-range interactions separately. The additional interactions with the solvent are contained in the V_0 term. The quantity V_0 represents the energy of a quasifree electron in the same medium.[8]

(1) Address correspondence to this author at the Department of Chemistry, Louisiana State University, Baton Rouge, La. 70803.
(2) D. A. Copeland, N. R. Kestner, and J. Jortner, *J. Chem. Phys.*, **53**, 1189 (1970).
(3) (a) K. Fueki, D. F. Feng, L. Kevan, and R. Christoffersen, *J. Phys. Chem.*, **75**, 2297 (1971); (b) D. F. Feng, K. Fueki, and L. Kevan, *J. Chem. Phys.*, **56**, 5351 (1972); **57**, 1253 (1972).
(4) L. Dorfman, *Proc. Colloq. Weyl III*, in press.
(5) J. Dye, M. G. DeBacker, and L. M. Dorfman, *J. Chem. Phys.*, **52**, 6251 (1970).
(6) L. M. Dorfman, F. Y. Jou, and R. Wageman, *Ber. Bunsenges. Phys. Chem.*, **75**, 681 (1971).
(7) R. Olinger and U. Schindewolf, *Ber. Bunsenges. Phys. Chem.*, **75**, 693 (1971).

(d) The energy to form the cavity will involve surface tension work, E_{ST}, hydrogen repulsions between solvent molecules, E_{HH}, dipole repulsions between solvent molecules in the first coordination layer, E_{dd}, pressure volume work, E_{PV}, and since we will use the adiabatic theory, an energy to polarize the medium.

The electron wave function $\psi_i(r)$ will be determined by the solution of the adiabatic equation (in atomic units)

$$(-\tfrac{1}{2}\nabla^2 + V(r))\psi_i(r) = W_i\psi_i(r) \qquad (1)$$

where the potential is

$$V(r) = -N\mu e/r_d^2 - \beta e^2/r_c \qquad (0 < r < R)$$

$$V(r) = -N\mu e/r_d^2 - \beta e^2/r_c + V_0 \qquad (R < r < r) \quad (2)$$

$$V(r) = -\beta e^2/r + V_0 \qquad (r_d < r)$$

The relevant coordinates are defined as in Figure 1. In this model (referred to as Model 3 in our previous paper[2]) r_d is the distance to the dipole from the center of the cavity and r_c is the distance to the start of the continuum which lies beyond the first coordination layer. In this model it is assumed that the parameter, V_0, the energy of the quasifree electron in the medium also represents the interaction of the electron with the molecules in the first layer beyond that due to inertial polarization effects and the small electronic polarization contribution.[9] V_0 is not known experimentally. It has been estimated as -0.5 eV in liquid ammonia,[10] but we shall report calculations for $V_0 = 0.5, 0.0,$ and -0.5 eV.

The value of the effective dipole moment, μ, is equal to

$$\mu = \mu_0 \cos \theta \qquad (3)$$

where θ is the angle between the radius vector and the dipole moment vector. In the calculations of this section we will assume that the cosine can be replaced by its average value which can be calculated by the Langevin function, i.e.

$$\langle \cos \theta \rangle = \coth \chi - \chi^{-1} \qquad (4)$$

$$\chi = \mu_0 e C/kTr_d^2 \qquad (5)$$

and C is the charge enclosed. When considering the ground state or any state arrived by a vertical (Franck–Condon) excitation C is that for the ground or 1s state, C_{1s}, which is

$$C_{1s} = \int_0^R |\psi_{1s}|^2 d^3\mathbf{r} \qquad (6)$$

This calculation will be referred to a temperature-dependent model since at each temperature a different equation is solved so that the potential (2) and the resulting configurational diagrams are temperature dependent. This approach slightly complicates matters, if one wishes to consider temperature dependent properties.

The total electronic energy for state i will be given by

$$E_{el}^i = W_i + S_i \qquad (7)$$

where the small polarization term is

$$S_i = -N\alpha C_i^2/r_d^4 - e\gamma_0 C_i^2/2r_c \qquad (8)$$

where C_i is the charge enclosed within radius R for the state i in question.

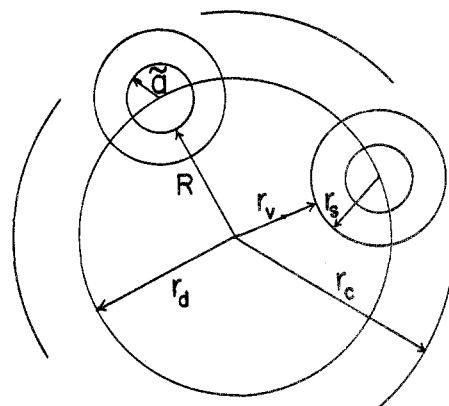The medium reorganization energy is the same as calculated in our earlier paper and outlined elsewhere.[2,11] It

Figure 1. Definitions of the distances involved in the molecular models. r_v is the void radius of the cavity, r_s is the effective solvent radius, and $\tilde{a}$ is the effective hard core of the molecules located at a distance r_d from the center of the cavity. The continuum begins at r_c (see ref 22).

is the sum of the terms listed above under item (d)

$$E_{mi} = E_{ST} + E_{HH} + E_{ddi} + E_{pv} + \pi \qquad (9)$$

One modification of the earlier work is the term E_{ddi}, the repulsion of the oriented dipoles.

$$E_{ddi} = \frac{D_N \mu_T^2}{r_d^3} \qquad (10)$$

where

$$\mu_T = \mu_0 \langle \cos \theta \rangle + e\alpha C_i/r_d^2 \qquad (11)$$

includes the correct induced dipole moment.[12] The constants, D_N, are listed in our earlier paper.[2] The hydrogen-hydrogen repulsion term is modified from earlier work[2] as

$$E_{HH} = C_{HH}^{(N)} \{\exp[-4.6(A_N R - B_N)] \langle \cos \theta \rangle\} \qquad (12)$$

where the constants are listed in ref 2.[13] The modification is in the last factor. This is added so that when $\langle \cos \theta \rangle$ goes to zero this contribution will vanish; i.e., the interactions will be the same as those in the bulk liquid. The remaining terms of eq 9 are evaluated as in ref 2 and 11.

In our calculations we assume that the 1s and 2p functions can be represented by single Slater type atomic orbitals whose exponents can be determined by the variational method. This choice is not ideal as the potential which traps the electron is very deep and near the center of the cavity resembles a particle in a box.[9,14] Nevertheless, at larger distances the potential is coulombic. The error in this approximation is calculated[9] to be about 10% for the ground-state energy. The general features of the results are not affected by this assumption. The electronic energy is minimized for a fixed temperature and then the polarization and medium reorganization energy terms are

(8) This quantity is presented in detail in the work on nonpolar fluids; e.g., B. E. Springett, M. H. Cohen, and J. Jortner, Phys. Rev., **159**, 183 (1967).

(9) An improved model has been used by A. Gaathon and J. Jortner (unpublished research). In that model two V_0 values are used, one in the first layer and another for the continuum. In that case electronic polarization with the first layer is not included separately. For ordinary liquid densities this improved model is similar to our results. In polar gases the results are quite different.

(10) A. Gaathon and J. Jortner, Proc. Colloq. Weyl III, in press, have a more accurate estimate of -0.22 eV for ammonia.

(11) J. Jortner, Ber. Bunsenges. Phys. Chem., **75**, 696 (1971).

(12) In ref 2, C_s is incorrectly written for C_i.

(13) In ref 2 there is another misprint in Table II for the constants in the hydrogen–hydrogen repulsion. A_6 should be 1.414 and B_6 should be 0.600.

(14) J. Logan and N. R. Kestner, J. Phys. Chem., **76**, 2738 (1972).

TABLE I: Results of Model 3 Calculations
One-Electron Cavity (Ammonia) (203°K)

	$V_0 = 0.5$ eV	$V_0 = 0.0$ eV	$V_0 = -0.5$ eV
$N = 4$			
E_t (= ΔH_1)	−0.537 eV	−0.909 eV	−1.30 eV
E_{el}	−1.668	−2.010	−2.404
R_0	−1.75 Å	1.75 Å	1.70 Å
$R_0^{eff\ a}$	3.1 Å	3.1 Å	3.0 Å
$h\nu$	1.16 eV	1.03 eV	0.94 eV
$N = 6$			
E_t	−0.678 eV	−0.972 eV	−1.294 eV
E_{el}	−2.069	−2.326	−2.603
R_0	2.20 Å	2.15 Å	2.15 Å
R_0^{eff}	3.1 Å	3.0 Å	3.0 Å
$h\nu$	1.30 eV	1.15 eV	0.99 eV

^{a} R_0^{eff} is the effective cavity radius measured by volume expansion experiments and $h\nu$ is the lowest allowed optical transition.

subsequently added. The optimum cavity size, R_0, is determined by minimizing the total energy

$$E_t^i(R) = E_{el}^i + E_{mi}(R) \tag{13}$$

so that

$$(\partial E_t/\partial R)_{R_0} = 0 \tag{14}$$

The results of these calculations at 203°K and for $N = 4$ and 6 are listed in Table I and plotted in Figures 2 and 3. These results supercede those published in ref 2. Logan and Kestner have also evaluated the first excited s type state (2s) of this system[14] obtained by vertical excitation from the ground state. It is shown in Figures 2 and 3 for comparison and labeled as the 2s curve.

In the above calculations we have evaluated the energy and properties of excited states as they arise in a Frank-Condon transition from the ground state; i.e., the inertial polarization of the first coordination layer and the continuum is fixed at the values appropriate for the charge density of the ground or 1s state. If the excited state is sufficiently long lived the inertial polarization could relax to a value appropriate for the equilibrium nuclear configuration of the excited state in question. We have evaluated the relaxed 2p states and the relaxed 1s state in which the inertial polarization is determined by the charge density of the relaxed 2p state. This means that in the average of cos θ and in μ_T we use the 2p charge density and the relaxed 2p wave functions. The results are summarized in Table IV where the maximum of the 2p → 1s emission is also listed. It is significantly red shifted from the absorption. The potential curves for these states are also shown in Figures 2 and 3 for two typical cases.

Also shown in Figures 1 and 2 are curves for the vertical continuum level, V_c, i.e., the energy of the quasifree electron if the cavity and medium have their inertial polarizations fixed at the values dictated by the charge density of the ground state.

$$V_C = E_{ST} + E_{HH} + E_{PV} + E_{dds} + \pi_s + V_0 \tag{15}$$

The curves represented by Figures 1 and 2 along with others to be presented below can now be used to study the details of electronic excitations as well as radiationless processes.

B. Temperature Independent Potentials—Two-Coordinate Model. In our previous work temperature has entered our calculations in two different ways. First of all, tem-
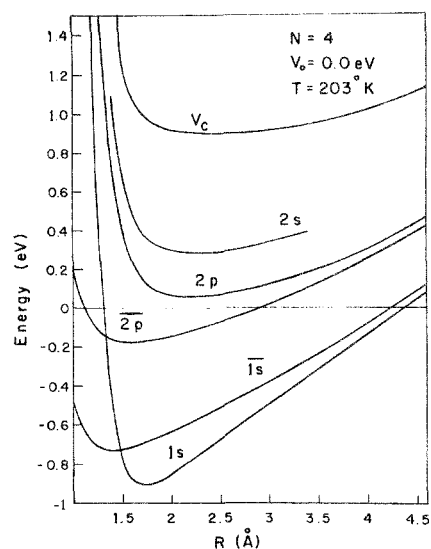
Figure 2. Configurational diagrams for the total energy as a function of the radius R for various electronic states when $N = 4$, $V_0 = 0.0$ eV, and $T = 203°$K. The ground state is denoted by 1s and the two bound excited states and the continuum level which exist when the polarization field is determined by the ground state are denoted by 2s, 2p, and V_c, respectively. The 2p state is the lowest energy P state when the polarization is determined by the 2p excited state, and the 1s state is the lowest energy level under the same polarization.

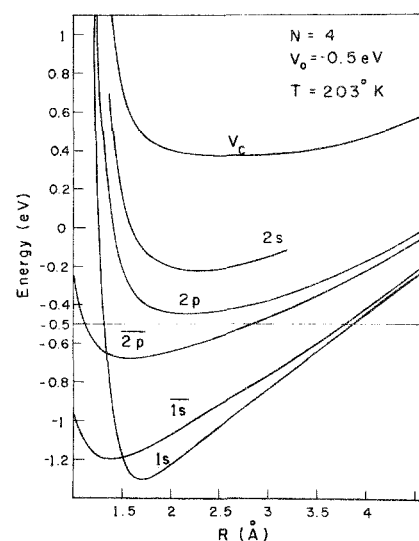**Figure 3.** Configurational diagrams for the total energy as a function of the radius R for various electronic states when $N = 4$, $V_0 = -0.5$ eV, and $T = 203°$K. The notation is the same as in Figure 2.

perature modifies the physical parameters characterizing the medium. Secondly, the electron-medium potential explicitly contains the temperature in that we use a temperature averaged cosine of the dipole orientation. The medium parameters change slowly with temperature whereas the average of the cosine changes rapidly. Thus it is advisable to advance a model in which temperature effects are kept out of the quantum mechanical calculation. One can always reintroduce thermal averages by the appropriate Boltzmann weighted average. In addition, however, one can consider the effects of the fluctuations in the cos θ term as they affect various properties.
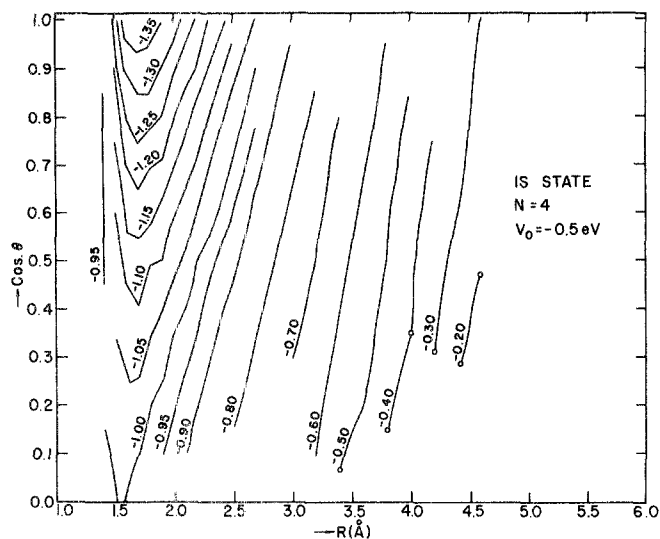
Figure 4. Configurational diagrams for the ground-state total energy as a function of R and θ. $N = 4$, $V_0 = -0.5$ eV. The numbers refer to constant potential surfaces in eV.
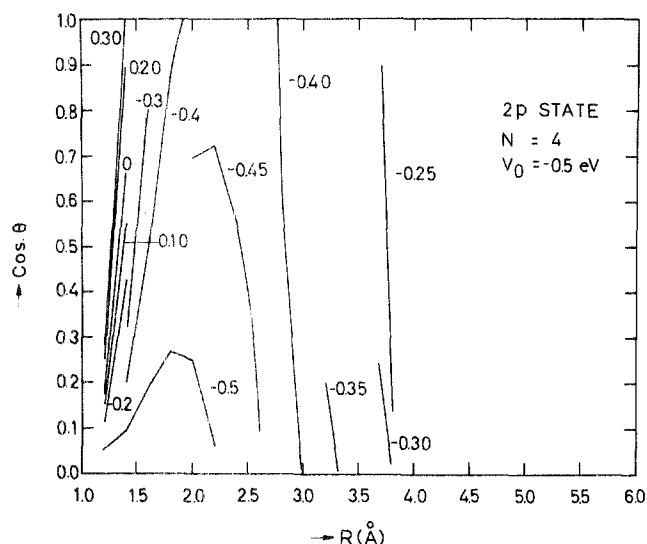

Figure 5. Configurational diagrams for the 2p excited state as a function of R and θ. Notation and parameters identical with those in Figure 4.

Figure 6. Temperature-independent potential model configuration diagrams for the total energy as a function of the radius R for $N = 4$ and $V_0 = -0.5$ eV. The last subscript now refers to the value of cos θ. Only curves for two values of cos θ are plotted. Each state has the bulk medium polarized according to its electron density (see text). The dots labeled 1s denote the temperature averaged result where $\langle\cos\theta\rangle_{1s} = 0.8$-$0.9$. V_M is the medium or continuum level.

Figure 7. An expanded view of the upper portions of Figure 7 including the completely oriented dipole curve for the continuum or medium level. The arrow indicates the position of the minimum for the 1s state.

It is a simple matter to extend our previous formalism for the calculation of temperature-independent energies. Instead of using the temperature averaged values of cos θ in eq 3, 11, and 12, we evaluate the energy as a function of both R and cos θ where cos θ can range from 0.0 to 1.0. Such potential energy surfaces (i.e., configurational coordinates) for the 1s and 2p states are displayed in Figures 4 and 5.

There is still one problem in defining how that energy is to be calculated since we have averaged the set of coordinates representing the medium quasi-polaron modes. The thermally average effect is included in β and their effective displacement is included in the π term. There is a choice as to what π value should be included with each energy state. We have included in the curves of Figures 6, 7, and 8 the value of π appropriate to the state in question. Thus the difference between curves do not represent vertical excitations in terms of the medium coordinates. To obtain vertical excitations from these curves one needs
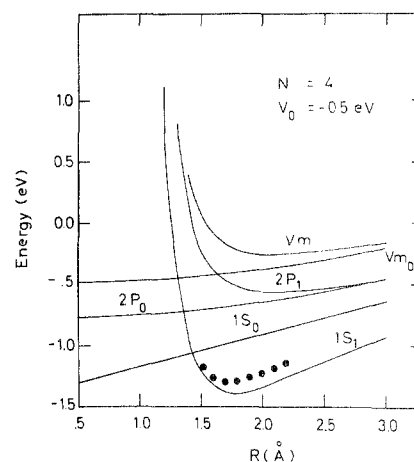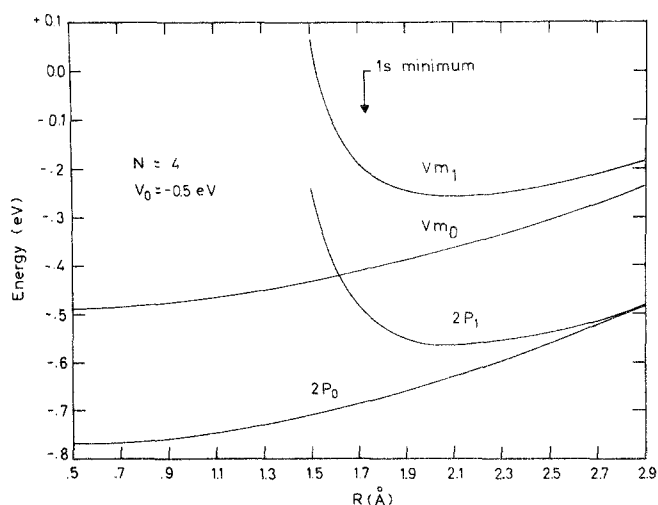
to correct for the difference in π values. Thus it is important to note that the 2p curves contain π_p calculated with 2p wave functions, the 1s curves contain π_s calculated with 1s functions, and the continuum or V_m curves do not contain any contribution of π. The last subscript on the curves refers to the value of cos θ. We have presented in Figures 6-8 only the cos $\theta = 0.0$ and cos $\theta = 1.0$ results. At small radii the one term wave function is inadequate. In addition, remember the π term is not the same for any two curves and for a vertical process they will be separated by the differences in the values of π appropriate to the various states and this is a few tenths of a volt.

To relate this to our previous work,[2] we must remember that before we used $\langle\cos\theta\rangle_{1s}$ for all Franck-Condon transitions. The value of $\langle\cos\theta\rangle_{1s}$ for the ground state is about 0.85. In Figure 6 we indicate for reference the position of the thermally averaged results for 1s versus $1s_1$.

The use of this temperature-independent potential to calculate the thermally averaged energy of the bound
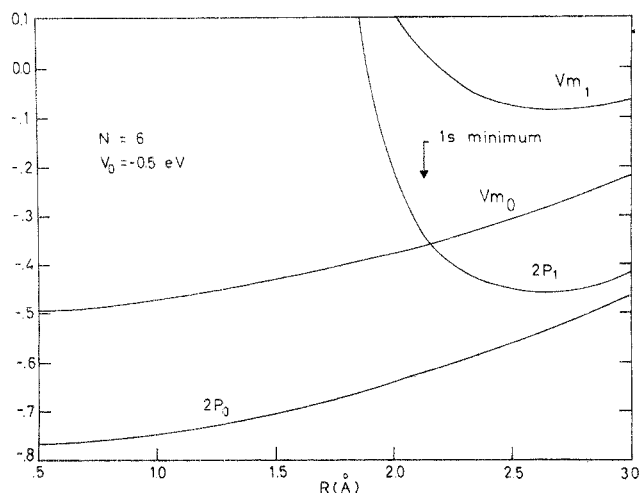
Figure 8. Temperature-independent potential model configuration diagrams for the total energy as a function of the radius R for $N = 6$ and $V_0 = -0.5$ eV. Notation is the same as in Figures 7 and 8.

states leads to almost exactly the same answers as in our previous calculation since for values of cos θ above about 0.6 the energy is a linear function of cos θ and thus averaging yields the same Langevin result as before. However, for weakly bound states and small values of cos θ this approximation is poor and thus the relaxed 2p states would probably change slightly if the proper averaging were done with a temperature-independent potential. It is unlikely that the *relative* behavior of the previous relaxed 2p and 1s states would change greatly.

III. Radiative Processes

A. Absorption Line Shape for the 1s → 2p Transition. In the previous section we have presented configuration diagrams for the ground (1s) and excited (2p) states of the solvated electron in ammonia. With these curves and a few reasonable assumptions we can calculate the line shape expected from this model. These assumptions are as follows. (a) The classical high-temperature limit for the absorption line shape can be safely used. This approximation implies that the relevant frequencies are lower than the thermal energies. The fundamental totally symmetric radial vibration of the electron cavity is about 80 cm^{-1}, while the characteristic frequencies of the medium modes are estimated[15] to be of the order of 1 cm^{-1}. Thus in the relevant temperature region 200–300°K this approximation is valid. (b) The semiclassical Condon approximation is invoked, whereupon the electronic transition moment is independent of the nuclear configuration. This is also reasonably good for the ranges of R considered (see section A4). The intensity distribution function, $F(E)$, for optical excitation at energy E for one configuration of the cavity can be recast in the general form

$$F(E) = \frac{|M|^2}{Z} \sum_\alpha \sum_\beta \exp(-\epsilon_\alpha / kT) \times$$
$$|\langle \chi_\alpha(\mathbf{X}) | \chi_\beta(\mathbf{X}) \rangle|^2 \delta(E + \epsilon_\alpha - \epsilon_\beta) \quad (16)$$

where M is the electronic transition moment, Z is the ground state partition function, and α and β represent the vibronic levels of the initial (1s) and the final (2p) states, respectively. These vibronic levels are characterized by the energies ϵ_α and ϵ_β and by the vibrational wave functions $\chi_\alpha(\mathbf{X})$ and $\chi_\beta(\mathbf{X})$, respectively. The generalized coor-

dinate $\mathbf{x}$ represents the set of the radical, R, and angular θ coordinates of the first coordination layer and the solvent polar modes $\{q\}$ outside this first layer whereupon $\mathbf{X} \equiv (R, \theta, \{q_k\})$.

Extensive theoretical studies have been performed[16,17] to derive explicit expression for the line shape function (16). General closed expressions can be derived only within the framework of the harmonic approximation which is inapplicable for the present problem as the potential surfaces for the R and θ coordinates exhibit large deviations from the harmonic model. However, in the high-temperature limit, Kubo and Toyozawa[17] have derived a general expression for the line shape which is valid for any set of potential surfaces

$$F(E) \frac{|M|^2}{Z} \int d\mathbf{X} \exp[-U_i(\mathbf{X})/kT] \times$$
$$\delta(E + U_i(\mathbf{X}) - U_f(\mathbf{X})) \quad (17)$$

where $U_i(\mathbf{X})$ and $U_f(\mathbf{X})$ correspond to the potential surfaces of the initial (1s) and the final (2p) electronic states. Thus, in the present case, we can write

$$F(E) = \frac{|M|^2}{Z} \int d\mathbf{X} \exp[-E_t^{1s}(\mathbf{X})/kT] \times$$
$$\delta(E + E_t^{1s}(\mathbf{X}) - E_t^{2p}(\mathbf{X})) \quad (17a)$$

Equation 17a demonstrates that in the high-temperature limit the radiative transition occurs at energies $E = E_T^{2p}(\mathbf{X}) - E_T^{1s}(\mathbf{X})$ in accordance with the classical Franck–Condon principle.

A1. One-Configurational Coordinate Model. Neglecting the role of the medium modes and utilizing the temperature dependent potential the energies $E_t^{1s}(\mathbf{X})$ and $E_t^{2p}(\mathbf{X})$ are a function of a single radial coordinate $\mathbf{X} \equiv R$, which corresponds to the cavity radius. We thus assume that the dependence of the energy on the nontotally symmetric vibrations is small and that the major contribution to the line width originates from the totally symmetric mode. In addition, the triply degenerate 2p electronic state is not split by this symmetric mode.

The line shape is now obtained from eq 17a in the form

$$A(E) = \frac{|M|^2}{Z} \exp[-E_t^{1s}(R)] \left| \frac{dR}{dE} \right| \quad (18)$$

In Figure 9 we show the results of one calculation of the line shape for a particular choice of parameters. This figure is similar to that of our earlier paper.[2] We include it in this paper in reference to the more detailed calculations to be presented below. The conclusions regarding this curve are the same as we presented earlier.[2] We have observed, however, that when cos θ is fixed at 1.0 rather than its thermal average the line shape is more asymmetric toward lower energies. This observation can be rationalized by noting that the cos θ dependence of the excited 2p state is very weak around cos $\theta \approx 1$. Thus by utilizing equation 17 for the medium one can show that the contribution of this mode to the line shape will result in a broadening only toward lower energies. This one coordinate (cos θ) line shape will be an exponentially decaying function with a width of $(\ln 2)kT$, which is quite small. Detailed numerical calculations presented in the next section confirm this qualitative conclusion.

(15) V. G. Levich, *Advan. Electrochem. Electrochem. Eng.*, **4**, 249 (1966).
(16) M. Lax, *J. Chem. Phys.*, **20**, 1752 (1952).
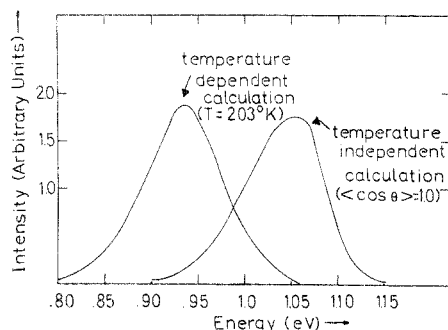(17) R. Kubo and Y. Toyozawa, *Progr. Theor. Phys.*, **13**, 160 (1955).

Figure 9. Optical lineshape for 1s → 2p transitions calculated from the potential dependent configurational diagrams with a single (R) mode. $N = 4$, $V_0 = -0.5$, and $T = 300°K$.

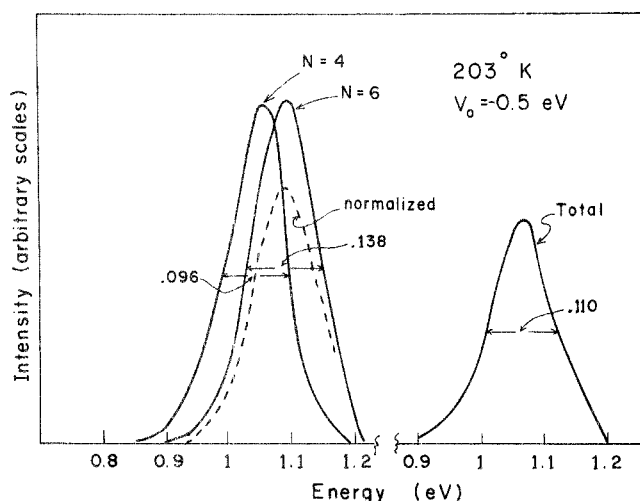**Figure 10.** Line shapes calculated at 203°K and $V_0 = -0.5$ eV by the temperature-independent two (R, θ) mode potential model. On the left are the line shapes for the $N = 4$ and $N = 6$ cavities including the $N = 6$ results normalized by its relative Boltzmann factor. On the right is the composite line shape obtained from the $N = 4$ and $N = 6$ cavities following eq 19 in the text.

A2. Two-Configurational Coordinates $(R, \cos \theta)$. In addition to the configurational coordinate, R, the cavity radius, it is very easy for us to study the dependence of another set of short range coordinates on the energy and line shape, namely $\cos \theta$. We will assume that the cavity is still spherical but that the dipole can move together in a way described by their collective coordinate, $\cos \theta$. It is now a simple matter to take the various potential curves and properly weight the transition energies, according to eq 17a. This was done for the absorption spectra by fitting the ground state energy and the excitation energy to a power series in $\cos \theta$ (a linear relation is sufficient for large values of $\cos \theta$).

On the left side of Figures 10 and 11 we have plotted line shapes for $N = 4$ and 6 and $V_0 = -0.5$ eV for two temperatures, 203 and 300°K. By comparing Figures 9 and 10 we see that the $\cos \theta$ mode results in small broadening at low energies and contributes little to the half-width. Within our curve fitting error of about ±0.004 eV we can see no effect on the half-width.

In Table I we see that the calculated ground state energy for the cavity with four and six coordination numbers are very similar. In our earlier work[2] it was also pointed out that the oscillator strengths of the two cavity models were similar.[18] With these conditions and our previous as-
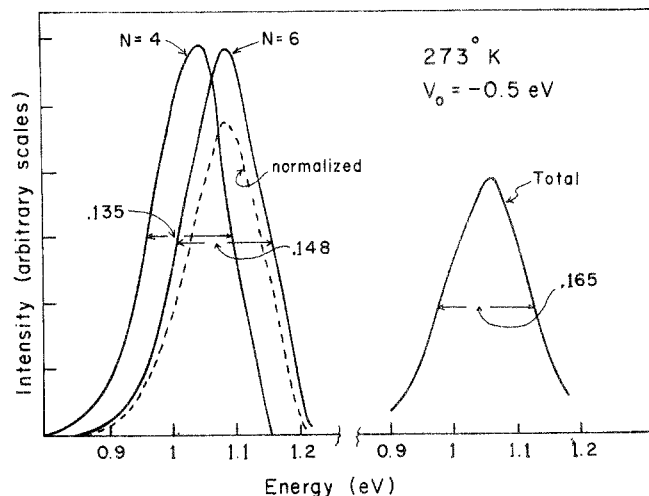

Figure 11. Line shapes calculated at 273°K and $V_0 = -0.5$ eV by the temperature independent two mode potential model. The notation is the same as in Figure 10.

sumptions we can write for the total expected compound line shape involving contributions for different short range configurations

$$F_T(E) = F_4(E) + \exp(-\Delta E°/kT) F_6(E) \qquad (19)$$

where $\Delta E°$ is the difference between the ground state energy for the 4 and 6 member cavities. This is calculated at the minimum of potential curves. In our two-coordinate model it is calculated at the radius corresponding to the lowest energy for $\cos \theta = 1.0$. On the right side of Figures 10 and 11 we plot the total line shape calculated by eq 19. In principle one should also add contributions for $N = 8$ but since it has a significantly higher total ground state energy in our model it would contribute very little.

A3. Role of Solvent Modes. Thus far we have neglected or rather suppressed another set of coordinates, namely the solvent polaron modes. These are included in our calculation in an average way *via* the β parameter in the potential and the π contribution. The general potential energy surfaces including the polaron modes can be recast by separating the long-range and the short-range nuclear displacements, so that

$$E_t^{1s}(\mathbf{X}) = f_{1s}(R,\theta) + g_{1s}(\mathbf{q}_\kappa) + E_t^{1s}(\mathbf{X}_0^{1s}) \qquad (20)$$

$$E_t^{2p}(\mathbf{X}) = f_{2p}(R,\theta) + g_{2p}(\mathbf{q}_\kappa) + E_t^{2p}(\mathbf{X}_0^{2p}) \qquad (21)$$

where the f and g functions describe the contribution of the first coordination layer and the medium to the total energy when these coordinates are displaced from their minima.

Following Levich we shall invoke two approximations to specify the contribution of the medium modes:[15] (a) the harmonic approximation whereupon small displacements of the medium modes are considered around the equilibrium configurations $\{q_\kappa°(1s)\}$ and $\{q_\kappa°(2p)\}$ in the two electronic states; (b) the medium modes will be approximated by the single mean frequency ω_0 in both electronic states. Qualitative estimates yield[19] $\hbar\omega_0 \approx 10^{12}$ sec$^{-1} \approx 1$ cm^{-1}.

(18) This is confirmed by unpublished calculations of A. Gaathon and J. Jortner. The previous values of the oscillator strengths published in ref 2 are in error due to a numerical error and the use of the dipole length formula. For further discussion see A. Gaathon, J. Jortner, and N. R. Kestner, *Chem. Phys. Lett.*, in press.
(19) R. Dogonadze, *Ber. Bunsenges. Phys. Chem.*, **75**, 628 (1971).

Thus we write

$$E_t^{1s}(\mathbf{X}) = f_{1s}(R,\theta) + \frac{\hbar\omega_0}{2}\sum_\kappa(q_\kappa - q_\kappa^\circ(1s))^2 +$$
$$E_t^{1s}(\mathbf{X}_0^{1s}) \quad (22)$$

$$E_t^{2p}(\mathbf{X}) = f_{2p}(R,\theta) + \frac{\hbar\omega_0}{2}\sum_\kappa(q_\kappa - q_\kappa^\circ(2p))^2 +$$
$$E_t^{2p}(\mathbf{X}_0^{2p}) \quad (23)$$

Defining a new set of medium polaron coordinates $Q_\kappa = q_\kappa - q_\kappa^\circ(1s)$ at reduced shifts of the minimum configuration $\delta\kappa = q_\kappa^\circ(1s) - q_\kappa^\circ(2p)$ we can write

$$E_t^{1s}(\mathbf{X}) = f_{1s}(R,\theta) + \frac{\hbar\omega_0}{2}\sum_\kappa Q_\kappa^2 \quad (24)$$

$$E_t^{2p}(\mathbf{X}) = f_{2p}(R,\theta) + \frac{\hbar\omega_0}{2}\sum_\kappa Q_\kappa^2 + \hbar\omega_0\sum_\kappa\delta_\kappa Q_\kappa$$
$$+ E_s + \Delta E \quad (25)$$

where the energy gap is

$$\Delta E = E_t^{2p}(\mathbf{X}_0^{2p}) - E_t^{1s}(\mathbf{X}_0^{1s}) \quad (26)$$

represents the difference between the energies of the two states at equilibrium nuclear configurations. We have also defined an energy (Stokes) shift

$$E_s = \frac{\hbar\omega_0}{2}\sum_\kappa\delta_\kappa^2 \quad (27)$$

Levich has shown[15] that E_s can be expressed in the form

$$E_s = \frac{1}{8\pi\beta}\int(D_s - D_p)^2\,dV \quad (28)$$

$$= 2\pi\beta\int(P_s - P_p)^2\,dV \quad (29)$$

where D_s and D_p are the electric displacement vectors in the s and p states while P_s and P_p are the corresponding polarizations of the two states.

It is possible to make some very rough statements concerning E_s. It behaves somewhat like the difference in the π term calculated using the 1s wave function and that calculated using the 2p wave function. Since we know these are two magnitudes similar, we expect E_s is small. To obtain a reliable value of E_s we have used the wave functions obtained to calculate D_s and D_p. For $N = 4$ and $V_0 = -0.5$ we obtain a value for E_s of 0.024 eV.

Focusing attention on the line shape (eq 17) we note that the factorization of the potential surfaces into short- and long-range contributions enables us to recast $F(E)$ in the form of a convolution. Neglecting the contribution of the θ mode (see section A3) we can write

$$F(E) = \int dR\Pi_\kappa dq_\kappa\int d\epsilon\,\exp[-f_{1s}(R)/kT] \times$$
$$\delta(E + f_{1s}(R) - f_{2p}(R) - \Delta E - \epsilon) \times$$
$$\exp[-\hbar\omega_0\sum_\kappa Q_\kappa^2/2kT]\,\delta(\epsilon - \hbar\omega_0\sum_\kappa Q_\kappa\delta_\kappa - E_s - \Delta E) \quad (30)$$

Defining the line shape functions for the two modes

$$\alpha(E - \epsilon) = \int dR\,\exp(-f_{1s}(R)/kT)\delta(E + f_{1s}(R) -$$
$$f_{2p}(R) - \epsilon) \quad (31)$$

$$\gamma(\epsilon) = \int\Pi_\kappa dq_\kappa\,\exp[-\hbar\omega_0\sum_\kappa Q_\kappa^2/2kT]\delta \times$$
$$(\epsilon - \hbar\omega_0\sum_\kappa\delta_\kappa Q_\kappa - E_s - \Delta E) \quad (32)$$

The line shape takes the form of a convolution

$$F(E) = \int d\epsilon\,\alpha(E - \epsilon)\gamma(\epsilon) \quad (33)$$

The line shape α originating from the radial cavity displacement was calculated previously and is given by

$$\alpha(E - \epsilon) = A(E - \epsilon) \quad (34)$$

where A is given by eq 18. The line shape (E) for the harmonic medium displacements can be easily evaluated utilizing the techniques of Kubo, Toyozawa,[17] and Lax[16] and is given by the Gaussian distribution

$$\gamma(\epsilon) = \exp\left[\frac{-(\epsilon - E_s - \Delta E)^2}{4kTE_s}\right] \quad (35)$$

The half-width of this distribution is given by

$$\Gamma_\gamma = 4(kTE_s\ln 2)^{1/2} \quad (36)$$

Numerical calculations yield for $V_0 = -0.5$ and $N = 4\Gamma_\gamma = 0.07$ eV. On the other hand, the width of the distribution $A(E - \epsilon)$ is $\Delta \approx 0.12$ eV at 300°K. As the A distribution can be reasonably well approximated by a Gaussian the total width, Γ, of the line shape (33) is given by the sum of the two widths

$$\Gamma \approx \Delta + \Gamma_\gamma = 0.19 \text{ eV} \quad (37)$$

We thus conclude that the contribution of the medium polaron modes to the line broadening of the bound–bound 1s → 2p transition is relatively important; however, it still cannot explain the discrepancy between theory and experiment.

A4. Conclusions and Other Possible Source of Line Broadening. Based on our calculations several general comments can be made. (1) Even though the calculated 1s → 2p absorption lines we have are quite broad they are narrower than the experimental widths by almost a numerical factor of 2. (2) The particular vibrational motion of the first coordination layer dipoles, namely cos θ, does not contribute significantly to line broadening. Almost all of the line shape arises from the spherically symmetric vibrations and from the long-range polaron modes. (3) The contribution of several types of cavities does contribute to line broadening but is not capable of leading to extremely wide lines. Furthermore, if this were the primary reason for broad line shapes then the half-width should be greatly dependent on the density of the fluid, and the best available data[10,20] for electrons in supercritical vapors suggest it is not the case. In the case of dense water vapor the line width does not vary greatly even when the gas density is reduced to 2% of the normal liquid water density.[10] (4) The theoretical line shapes are slightly asymmetric on the low-energy side while the experimental results are very skewed towards high energy. This asymmetry originates from the contribution of the θ mode. This slight low-energy asymmetry is removed if one properly includes the variation of the oscillator strength across the band. This variation of the oscillator strength across the band is about 30% and it will produce a more symmetrical line of almost the same width. (5) The theoretical line widths behave as $(T)^{1/2}$ contrary to experimental data[21] which show

(20) R. Olinger, U. Schindewolf, A. Gaathon, and J. Jortner, *Ber. Bunsen-ges. Phys. Chem.,* **75,** 690 (1971).

(21) D. F. Burrow and J. J. Lagowski, *Advan. Chem. Ser.,* **No. 50,** 125 (1965). I. Hurley, T. R. Tuttle, Jr., and S. Golden, "Metal Ammonia Solutions," J. J. Lagowski and M. J. Sienko, Ed., Butterworths, London, 1970.

a much weaker temperature dependence in dilute metal ammonia solutions.

The final comparison between the latest theoretical and experimental results are summarized in Figure 12. The fact that the maxima of the two curves do not agree is not important, but their great difference of shapes is crucial. There are many possible explanations for this qualitative discrepancy.

First of all, it is possible that our model is not accurate enough especially with regard to the small differences between the $N = 4$ and $N = 6$ cavities. This is possible but rather unlikely since no matter what relative energies are assigned to the two species the observed spectra cannot be duplicated. For example, if they are moved far apart the composite spectrum will have a dip between the two peaks.

Another explanation commonly proposed is that the high energy tail of the absorption involves higher excited states (3p, 4p, even continuum levels). Within our model this can also be ruled out. The higher excited states should have electronic energies given by a Rydberg-like formula

$$E_n = -\frac{\beta^2}{2n^2} + V_0 \qquad (38)$$

This works well even for the 2p state and should be even better for the 3p and 4p levels. Using eq 38 we can locate the 1s → 3p and 1s → 4p transitions relative to the 1s → 2p transition. However, as shown in Figure 12 these lie at very high energies and in order to explain the experimental data even approximately they would have to be extremely broad and carry an extremely large oscillator strength. From the calculation of all previously considered line broadening factors it is unlikely that they would have half-widths over 0.4 eV. Other calculations indicate that the oscillator strength available to all excited states beyond 2p is small.[18] These excited levels should also be greatly affected by the density of the fluid since they depend directly on β and yet lines in very low density water vapor[10] are as broad as those in the liquid. Also, Lugo and Delahay[22] were not successful in a phenomenological fitting the solvated electron spectrum with up to four gaussian distributions. These remarks apply to water and ammonia.

Thus the question of the extremely broad lines remains. Two other explanations have been proposed which have not been fully evaluated as yet.

Thus far we have assumed spherical cavities with spherically symmetrical vibrations. Asymmetric fluctuations might lead to an appreciable increase in the half-width. However, the 2p excited state energy is almost independent of any nonspherical vibrations of the first coordination layer and since the estimates indicate that asymmetric modes have a very small force constant one calculates that *at most* they could contribute $kT \ln 2$ or 0.012 eV to the half-width. Less well understood is the Jahn–Teller effect on the line shape but in any case it will lead to asymmetric lines and increase the width as $\sqrt{T}$,[23] both ideas contrary to experimental data.

Another possible explanation of the line shape is a permanent distortion of the cavity from its spherical shape. It is hard to justify such a model but it could arise from the rapid exchange of solvent molecules between the first coordination layer and the bulk medium. At any one instant one would have a variety of cavity shapes. The average would be represented by our model but large deviations from it would be possible. This was considered for
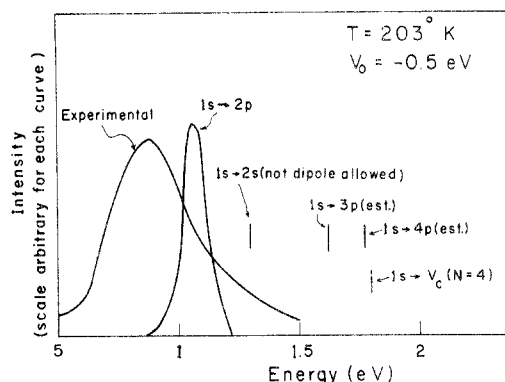

Figure 12. Typical transition energies and line shapes obtained from these models in comparison with typical experimental data. The 1s → 2p line shape is the total curve in Figure 10. The other lines indicate where the various bound–bound and bound–continuum (1s → V_0) levels are located for this model. These curves incorporate the contribution of the short-range R and θ displacements, disregarding the role of the long range polaron displacements.

TABLE II: Metal–Ammonia Solutions Relaxed States at 203°K

	$V_0 = 0.5$ eV	$V_0 = 0.0$ eV	$V_0 = -0.5$ eV
		$N = 4$	
E_t ($\overline{2p}$)	0.3160 eV	−0.1826	−0.6811 eV
$h\nu$ (emission)	0.594 eV	0.548 eV	0.506 eV
E_t ($\overline{1s}$)	−0.2780 eV	−0.7301 eV	−1.1873 eV
R	1.55 Å	1.55 Å	1.55 Å
C_s	0.197	0.09	0.08
C_p	0.007	0.007	0.007
		$N = 6$	
E_t ($\overline{2p}$)	0.3839 eV	−0.1126	−0.6093 eV
$h\nu$ (emission)	0.627 eV	0.535 eV	0.467 eV
E_t ($\overline{1s}$)	−0.2429 eV	−0.6477 eV	−1.0765 eV
R	2.05 Å	2.05 Å	2.00 Å
C_s	0.181	0.153	0.126
C_p	0.020	0.019	0.017

the case of electrons in helium.[24] Although we cannot treat this problem easily without major variations in our model, one can argue that this could lead to asymmetric lines if nonspherical cavities had larger transition energies, becoming slightly more asymmetric at higher temperatures (for the case where density is constant), and total half line widths increasing more slowly than $\sqrt{T}$ due to the many contributions to the total line shape. It would suggest that lines in dense polar fluids could be as broad as those in polar liquids. However, although there is evidence for all these predictions, in the absence of quantitative evidence all of this is speculation. At the moment we cannot see how to calculate any of these features from first principles.

B. Emission Line Shapes (2p → 1s). If the 2p state exists long enough for the medium to relax to the new charge density, then it may be possible to see an emission from the relaxed 2p level to the relaxed 1s level. The energies of such states were given in Table II. Using the curves

(22) R. Lugo and P. Delahay, *J. Chem. Phys.*, **57**, 2122 (1972). Note, however, that this present paper emphasizes the need to use different line widths for the bound–bound and bound–continuum transitions.

(23) Y. Toyozawa in "Dynamical Processes in Solid State Optics," R. Kubo, Ed., Benjamin, New York, N. Y., 1969.

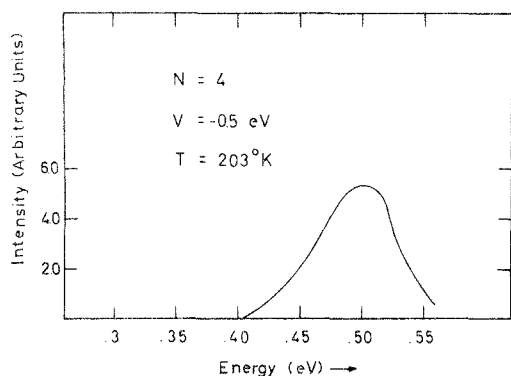(24) B. Fowler and D. L. Dexter, *Phys. Rev.*, **176**, 337 (1968).

Figure 13. 2p $\rightarrow$ 1s emission line shape calculated from the temperature-dependent one-mode model.

of Figure 3 it is possible to calculate using formulas 16–18 the emission line shape inverting the sign of E in the δ function. The only change is that $A(x)$ refers to points on the relaxed 2p configuration curves. The resulting line shape is plotted in Figure 13. It is again quite broad, especially considering the very low energy of the emission. The emission is Stokes shifted about 0.4 eV to the red from the absorption. This emission would be extremely interesting if it could be observed since it could have a rather different line shape from the absorption as the emitting state has a very different electronic structure.

C. Photoionization. Using the calculated curves for the energy of various states we can calculate the photoionization profile[25,26] as a function of the photon energy. This calculation differs from that in the previous section in two ways: first of all, there are additional line broadening effects and secondly we cannot invoke the Condon approximation and remove the energy dependence of the transition matrix element or cross section from the integral over all possible configurational states. Thus we need to evaluate the following integral

$$L(\nu) = \int \sigma(\nu, \nu_1) F(\nu_1) \, d\nu_1 \qquad (39)$$

where $F(\nu_1)$ is related to the quantity we have calculated in the previous section and it is proportional to the line shape if one can neglect the energy dependence of the cross section or transition matrix element σ. The reason for the integral is that a photon of energy ν can ionize all configurations with energy less than ν. To reduce this result to the previous case we not only factor out σ but replace it with a δ function since $F(\nu_1)$ contains all contributions of energy E which is equal in that case to ν.

In our considerations $F(\nu_1)$ represents the probability for finding states with an ionization energy ν_1 at a temperature T. The ionization energy is evaluated as

$$\nu_1 = E_c(R) - E_t^{1s}(R) \qquad (40)$$

i.e., the difference between the total energy of the continuum and the total energy of the ground state. In Table III we present values for this quantity at the most probable radius as determined by our temperature dependent calculations.

Using the same procedure as in the previous section we evaluate the $F(\nu_1)$ including the contributions from the symmetric vibration, *i.e.,* changes in R. The results are very similar to those for the 1s $\rightarrow$ 2p transition and we shall use those values here. In addition, however, we must consider the effect of broadening by polaron modes. This

TABLE III: The 1s Continuum Thresholds for the Most Stable Cavity Radius (Using Temperature-Dependent Model and $T = 203°K$)

	$V_0 = 0.5$ eV	$V_0 = 0.0$ eV	$V_0 = -0.5$ eV
$N = 4$	2.071 eV	1.976 eV	1.846 eV
$N = 6$	2.364 eV	2.138 eV	2.004 eV
$N = 8$	2.461 eV	2.164 eV	1.890 eV

is a very small contribution for bound–bound states (especially for the 1s $\rightarrow$ 2p transition) but it is large for bound–continuum transitions since the electric displacement in the continuum states is zero and thus in eq 28 the value of E_s is simply the value of π_s for the ground state. This value is 0.78 eV for $N = 4$ and $V_0 = -0.5$ eV. Substituting this value into eq 36 we find an additional line broadening of 0.388 eV. If the two contributions are independent we predict at $T = 203°K$ a line half-width for the transition of 0.096 + 0.388 = 0.484 eV. For the $N = 6$ cavity and $V_0 = -0.5$ eV we obtain 0.138 + 0.369 = 0.507 eV since the value of π is 0.75 eV.

If we assume a Gaussian distribution we can write an explicit expression for $F(\nu_1)$ in terms of the half-width, w, using the notation of Delahay.[26]

$$F(\nu_1) = \exp(-y^2) \qquad (41)$$

where

$$y = \frac{1.665}{w}(\nu_1 - \nu_1(R_0)) \qquad (42)$$

where $\nu_1(R_0)$ is tabulated in Table III. The temperature dependence is contained in the half-width which was found theoretically to vary as $\sqrt{T}$ thus further justifying eq 26.

More complicated is the calculation of the energy-dependent cross section. This is dependent on the square of a matrix element of the form

$$\langle \psi_i | \vec{r} | \psi_f \rangle \qquad (43)$$

in the dipole length formulation. ψ_i and ψ_f are the initial and final state wave functions. We have a good idea of the initial wave function but we have only approximate ideas of the form of ψ_f. We notice, however, that this matrix element involves radial integrals of the form

$$\int \psi_i^* r^3 \psi_f \, dr \qquad (44)$$

and thus they are very dependent on the behavior of the wave functions at larger r. Furthermore, ψ_f by symmetry must have orbital angular momentum $l = 1$. We have already seen that even the 2p state is well approximated by a purely Coulombic potential with its long-range behavior. Therefore in order to get the proper energy dependence of the cross section we can use the exact formulas appropriate to a hydrogen atom (or a screened hydrogen-like atom) as derived in Bethe and Saltpeter.[27] Except for some constants the results are proportional to

$$\sigma(\nu_1 \nu) = \nu_1^3 \nu^{-4} f(\nu/\nu_1) \qquad (45)$$

where

$$F(\nu/\nu_1) = 1 + \frac{4}{3}\left(\frac{(\nu - \nu_1)}{\nu_1}\right) = \frac{4}{3}\left(\frac{\nu}{\nu_1}\right) - \frac{1}{3} \qquad (46)$$

if

(25) J. Häsing, *Ann. Phys.* **37**, 509 (1940).
(26) P. Delahay, *J. Chem. Phys.*, **55**, 4188 (1971).
(27) H. A. Bethe and E. E. Saltpeter, "Quantum Mechanics of One- and Two-Electron Atoms," Academic Press, New York, N. Y., 1957, pp 303–308.

$$(\nu - \nu_1) < \sqrt{3}\,\nu_1$$

or so.

For very small $(\nu/\nu_1 - 1) < 0.2$ or so, this result has often been expanded as

$$F(\nu/\nu_1) = (\nu/\nu_1)^{4/3} \qquad (47)$$

leading to a cross section varying as

$$\sigma(\nu_1,\nu) = \frac{1}{\nu_1}(\nu_1/\nu)^{8/3} \qquad (48)$$

except for the $(1/\nu_1)$ factor this is in the form used by Delahay.[28] Delahay was able to very nicely express $L(\nu)$ in terms of the line width and the maximum of the line, $\nu_1(R_0)$.[26] Because he used the $\frac{8}{3}$ power expression he had to evaluate the integrals numerically. We will show now that if we use the full low-energy expressions (45) and (46) one can evaluate the answer analytically and in the case of reasonable line widths obtain a very simple expression.

Because the photoionization profiles are of interest to many people we will present our derivation in some detail. Following Appendix A in Delahay's paper,[26] we can express eq 39 using eq 41, 42, 45, and 46 as

$$L(z_{\rm p}) = \frac{4}{3}y_c(|1 + z_{\rm p}|)^{-3}\int_{-1}^{z_{\rm p}}(|1 + z|)^2\,\exp(-z^2 y_c^2)\,dz -$$

$$\frac{1}{3}y_c(|1 + z_{\rm p}|)^{-4}\int_{-1}^{z_{\rm p}}(|1 + z_{\rm p}|)^2\,\exp(-z^2 y_c^2)\,dz \qquad (49)$$

using Delahay's notation in terms of our parameters

$$y_c = \left(\frac{1.665}{w}\right)\nu_1(R_0) \qquad (50a)$$

and

$$z_{\rm p} = \frac{\nu_1 - \nu_1(R_0)}{\nu_1(R_0)} \qquad (50b)$$

The integrals in eq 49 can be evaluated in terms of error functions and their derivatives as well as ordinary exponential integrals (for odd powers of z). To carry out the analysis one must perform a separate calculation for $z_{\rm p} > 0$ and for $z_{\rm p} < 0$, as the functional dependence is quite different in the two regions. To simplify the result we shall define

$$\Phi(x) \equiv \mathrm{erf}(x) = \frac{\sqrt{\pi}}{2}\int_0^x e^{-t^2}\,dt$$

furthermore
$$\Phi'(t) = d\Phi/dx|_{x=t} \qquad (51)$$

$$(\sqrt{\pi}/2)\,\Phi'(t) = e^{-t^2}$$

For $z_{\rm p} < 0$ we find

$$P(z_{\rm p}) = \frac{2}{\sqrt{\pi}}L(z_{\rm p}) = \frac{4}{3}(1 + z_{\rm p})^{-3}\{(1 + (2y_c^2)^{-1}[\Phi(y_c) +$$

$$\Phi(y_c z_{\rm p})] - (2y_c)^{-1}[\Phi'(y_c) + z_{\rm p}\Phi'(y_c z_{\rm p})] +$$

$$\Phi'(y_c)(y_c^{-1} + y_c^{-3}) - \Phi'(y_c z_{\rm p})(z_{\rm p}^2 y_c^{-1} + y_c^{-3})\} -$$

$$\frac{1}{3}(1 + z_{\rm p})^{-4}\{(1 + (\tfrac{3}{2})y_c^{-2})[\Phi(y_c) + \Phi(y_c z_{\rm p})] -$$

$$(\tfrac{3}{2})y_c^{-1}[\Phi'(y_c) + z_{\rm p}\Phi'(y_c z_{\rm p})] + (\tfrac{3}{2})\Phi'(y_c)(y_c^{-1} + y^{-3}) -$$

$$(\tfrac{3}{2})\Phi'(y_c z_{\rm p})[z_{\rm p}^2 y_c^{-1} + y_c^{-3}] + \Phi'(y_c)y_c^{-5}[1 + (y_c^2 y_c^4)/2] -$$

$$\Phi'(y_c z_{\rm p})y_c^{-5}[1 + y_c^2 z_{\rm p}^2 + (z_{\rm p}^4 y_c^4)/2] \qquad (52)$$

For $z_{\rm p} = 0$ we obtain

$$P(0) = \Phi(y_c)[1 + (\tfrac{1}{6})y_c^{-2}] - (\tfrac{5}{6})y_c^{-3} + (\tfrac{1}{3})y_c^{-5} +$$

$$\Phi'(y_c)[(\tfrac{1}{2})y_c^{-1} + (\tfrac{1}{2})y_c^{-3} - (\tfrac{1}{3})y_c^{-5}] \qquad (53)$$

The expression for $z_{\rm p} < 0$ is given in Appendix I.

Before proceeding with our calculations it is important to estimate the size of our parameters. We have $\nu_1(R_0) \approx 2$ eV, $W \sim 0.5$ eV, so $y_c \sim (1.7)(2)/0.5 \sim 6.6$. Also from the calculations of Delahay[26] we know that the integration changes very rapidly for values of $z_{\rm p}$ around zero; for $z_{\rm p} > 0.5$ or so the integral is almost constant. In addition, for $z_{\rm p} < 0.5$ the answer is almost zero. These values suggest that some very important approximations can be made since $y \geq 5$. In this limit we can neglect to within a few per cent erf(y^{-2}) vs. 1 and e^{-y^2} vs. 1, or $\Phi'(y)$ vs. 1.

These results greatly simplify the expressions. Consider $P(0)$ in these limits

$$P(0) \approx \Phi(y_c)[1 + (\tfrac{1}{6})y_c^{-2}] - (\tfrac{5}{6})y_c^{-3} \simeq 1.00 \qquad (54)$$

to about three significant figures for $y \geq 5$.

Likewise for the other limits we obtain

$$P(z_{\rm p} > 0) = \frac{4}{3}(1 + z_{\rm p})^{-3}[1 + \Phi(y_c z_{\rm p}) - \Phi'(y_c z_{\rm p})((\tfrac{1}{2})z_{\rm p}y_c^{-1} +$$

$$z_{\rm p}^2 y_c^{-1} + y_c^{-3})] - (\tfrac{1}{3})(1 + z_{\rm p})^{-4}[1 + \Phi(y_c z_{\rm p}) -$$

$$\Phi'(y_c z_{\rm p})(\tfrac{3}{2})z_{\rm p}y_c^{-1} + (\tfrac{3}{2})z_{\rm p}y_c^{-1} + 3y_c^{-3} + y_c^{-5} +$$

$$z_{\rm p}^2 y_c^{-3} + (z_{\rm p}^4 y_c^{-1})/2) \qquad (55)$$

$$P(z_{\rm p} < 0) = \frac{4}{3}(1 - \eta_{\rm p})^{-3}\{1 - \Phi'(y_c\eta_{\rm p})[\eta_{\rm p}^2 y_c^{-1} +$$

$$y_c^{-3} - (\tfrac{1}{2})\eta_{\rm p}y_c^{-1}] - \Phi(y_c\eta_{\rm p})\} -$$

$$\frac{1}{3}(1 - \eta_{\rm p})^{-4}\{1 - \Phi(y_c\eta_{\rm p}) - \Phi'(y_c\eta_{\rm p})[(\tfrac{3}{2})\eta_{\rm p}^2 y_c^{-1} +$$

$$y_c^{-3} - (\tfrac{3}{2})\eta_{\rm p}y_c^{-1} + y_c^{-5} + \eta_{\rm p}^2 y_c^{-3} + (\tfrac{1}{2})\eta_{\rm p}^4 y_c^{-1}]\} \qquad (56)$$

where $n_{\rm p} = -z_{\rm p} > 0$, but less than 1.0.

For the regions of interest it was found that terms involving $\Phi'(y_c\eta_{\rm p})$ are very small (3 parts in 1000 or less) and thus very reliable, very simple expressions can be used over all regions of $z_{\rm p}$.

$$P(z_{\rm p} > 0) = (1 + z_{\rm p})^{-3}[(\tfrac{4}{3}) - (\tfrac{1}{3})(1 + z_{\rm p})^{-1}] \times$$
$$[1 + \Phi(y_c z_{\rm p})] \qquad (57)$$

$$P(z_{\rm p} < 0) = (1 + z_{\rm p})^{-3}[(\tfrac{4}{3}) - (\tfrac{1}{3})(1 + z_{\rm p})^{-1}] \times$$
$$[1 - \Phi(y_c z_{\rm p})] \qquad (58)$$

$$P(z_{\rm p} > 0) = [1 - (\tfrac{8}{3})z_{\rm p} + (\tfrac{14}{3})z_{\rm p}^2][1 + \Phi(y_c z_{\rm p})] \qquad (59)$$

(when $z_{\rm p} < 0.5$).

The region in which the asymptotic result holds is therefore when $\Phi(y_c z_{\rm p}) \sim 1$. The exact limit depends on the precision required. This simple result occurs because of the large value of y in the present examples. In that case

$$\int_{-1}^{z_{\rm p}}(1 + z)^n e^{-y_c^2 z^2}\,dz \approx \int_{-1}^{z_{\rm p}}e^{-y_c^2 z^2}\,dz \qquad (60)$$

since only small values of z contribute to the integral. Thus the integral depends very weakly on the power of n. Therefore, the results of Delahay at large y_c are equivalent to the above calculations. For small values of y_c both our approximate formulas (eq 57-59) and those of Delahay need further corrections. In that case the complete expressions of eq 52, 53, and Appendix A are required.

(28) P. Delahay (ref 26) neglected to include the ionization potential contained in the factor in front of eq 71.11 of ref 27. His results in his Appendix A are thus slightly narrower than our calculations. However, for large values of y, i.e., narrow lines, the integral is almost independent of the specific power law and thus his results are good. See eq 60.
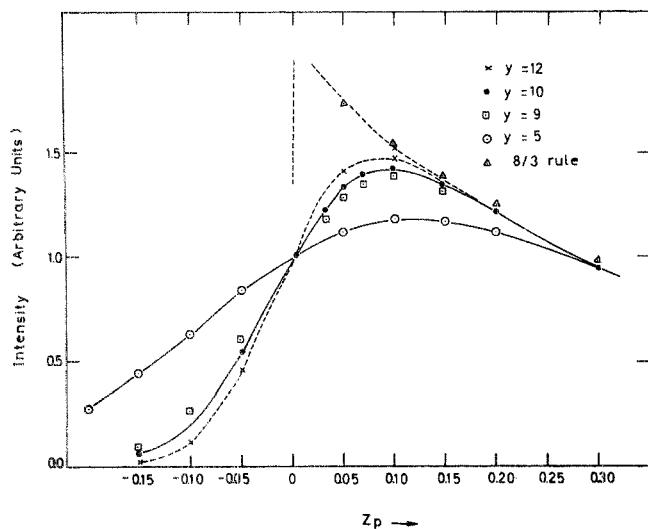
Figure 14. Photoemission profiles calculated for various values of y_c.

Figure 15. Predicted photoionization line shape for the solvated election in liquid ammonia.

In Figure 14 we present the reduced plots of the photoionization energy profile for various values of y in the region of interest. The points were calculated using the expressions 39 and 40 but in most cases, eq 57 and 58 yield results within a per cent or so of these answers. We have also plotted the asymptotic behavior which departs significantly from the integrated result for $z_p < 0.1$ when $y_c \sim 10$ and for $z_p < 0.2$ when $y_c \sim 5$. The points marked A are for the $8/3$ low asymptotic behavior. It differs very little from the complete result for $z_p < 0.3$.

Since our calculations indicate that both $N = 4$ and $N = 6$ cavities are energetically stable we have calculated the total contribution (unnormalized) from both cavities at a temperature corresponding to about 240°K. This is plotted in Figure 15 for suitable parameters. For the $N = 4$ state we used $\nu_1(R_0)$ from Table III for $T = 203°K$ and $V_0 = -0.5$ eV and $y = 5$ for a reasonable line width at 240°K. For $N = 6$ we also used $y = 5$, the corresponding energy from Table III and a weighting factor of 0.8 relative to the $N = 4$ case. It is apparent that with several cavity types the profile is very broad and very complicated. For values of $z_p > 0.2$ the total result behaves as if the ionization potential were 1.9 eV and not either 1.85 or 2.00 eV. In general no simple power law behavior is expected to work.

The only data with which we can compare our results is the photoelectron emission spectrum of metal–ammonia solutions of Häsing.[25] To apply our calculations to that case involves some drastic assumptions but if we assume that this spectrum behaves as $E^{-8/3}$ down to 2 eV and if extrapolated to zero current in that way one obtains 1.85 eV. Our curve in Figure 15 deviates from any simple law
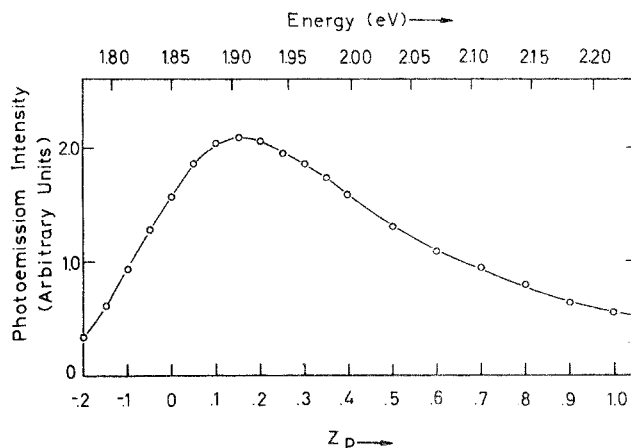
in the region near the maximum or at about 2.2 eV, but again we emphasize that these interpretations are risky and one needs direct measurements of the photoionization. More experimental data is desperately needed.

It has been suggested that the high energy tail of the optical absorption is in fact the bound–continuum transition.[26] Delahay has even analyzed the spectra of hydrated electron and electrons in 3-MP, THF, and HMPA in terms of such an assumption. They obey an $E^{-8/3}$ plot. However, the calculations presented in section A suggest that the high energy tail in these cases may not necessarily be part of the bound–continuum transition. (For further evidence in the last two cases, see ref 22.) It is also important to note that if several types of cavities with different $E_1(R_0)$ contribute the true photoemission line profile, it will very likely not have a simple $E^{-8/3}$ or any other power law dependence except at extremely high energies where only the highest value of $\nu_1(R_0)$ remains important. Unfortunately, the experimental data are not yet available to check on this feature.

Appendix

Total Expression for $P(z_p < 0)$. Using the notation of eq 56 and setting $\eta_p = -z_p$ for $z_p < 0$, we find

$$P(z_p < 0) = \frac{4}{3}(1 - \eta_p)^{-3}\{(1 + (\tfrac{1}{2})y_c^{-2})(\Phi(y_c) -$$

$$\Phi(y_c\eta_p)) + \Phi'(y_c)(y_c^{-3} + (\tfrac{1}{2})y_c^{-1}) - \Phi'(y_c\eta_p)[\eta_p^2 y_c^{-1} +$$

$$y_c^{-3} - (\eta_p/2)y_c^{-1}]\} - \frac{1}{3}(1 - \eta_p)^{-4}\{(1 + (\tfrac{3}{2})y_c^{-2})[\Phi(y_c) -$$

$$\Phi(y_c\eta_p)] + \Phi'(y_c)[(\tfrac{3}{2})y_c^{-3} + y_c^{-5}(1 + y_c^2 + y_c^4/2)] -$$

$$\Phi'(y_c\eta_p)[(\tfrac{3}{2})\eta_p^2 y_c^{-1} + (\tfrac{3}{2})y_c^{-3} + y_c^{-5}(1 + \eta_p^2 y_c^2 +$$

$$(\tfrac{1}{2})y_c^2\eta_p^4) - (\tfrac{3}{2})\eta_p y_c^{-1}]\}$$